Research Article

Ultrafast Laser-Ablated Bioinspired Hydrogel-Based Porous Gating System for Sustained Drug Release

Juan Zhang, Bingrui Liu,* Chao Chen, Shaojun Jiang, Yiyuan Zhang, Bing Xu, Ang Li, Junchao Xu, Dawei Wang, Leran Zhang, Yanlei Hu, Jiawen Li, Dong Wu, Jiaru Chu, and Zuojun Shen*

Cite This: ACS Appl. Mater. Interfaces 2022, 14, 35366−35375

Read Online

ACCESS | 📊 Metrics & More | 📖 Article Recommendations | 🆂 Supporting Information

ABSTRACT: Gating systems have been extensively researched in energy harvesting, lab-on-chip applications, and so forth. However, the controlled drug delivery system with artificial hydrogel-based porous gating systems (HPGSs) is rarely reported. Herein, a biomimetic HPGS with a pH-responsive hydrogel as the valve and polydimethylsiloxane as the frame is fabricated by in situ femtosecond laser microdrilling and subsequent ultraviolet exposure. The proposed HPGS loaded with doxorubicin hydrochloride (DOX) is stable under physiological conditions, has a low drug leakage rate, and can achieve sustained drug release in a low pH environment. The experimental results show that the drug release is mainly controlled by non-Fickian diffusion, which renders the dynamic speed control of molecular transport possible.

Moreover, the HPGS can also be prepared into an antitumor microcapsule. The results of in vitro cell experiments demonstrate that DOX@HPGS can release drugs and achieve terrific therapeutic efficacy in the elimination of HeLa cells in the acidic environments around tumor cells. This functional HPGS is envisioned to be an ideal pH-response carrier for sustained drug release treatment of digestive diseases such as inflammatory bowel disease and gastrointestinal cancer.

KEYWORDS: femtosecond laser, micro/nanofabrication, sustained drug release, intelligent gating system, pH-responsive hydrogel
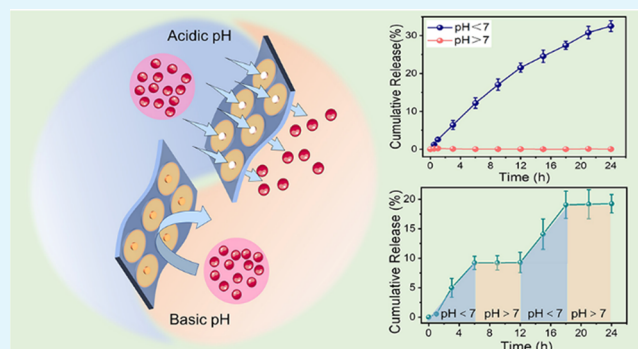
INTRODUCTION

In the past decade, intelligent porous gating systems with high selectivity and subtle triggering have been extensively explored in energy harvesting, water treatment, soft robotics, and so forth.[1,2] Accordingly, by artificially fabricating porous frames and developing stimuli-triggered materials as valves, a variety of intelligence-based smart gating systems have been designed that respond to external stimuli such as light irradiation, magnetic fields, temperature, or mechanical strain, aiming to achieve dynamic control of fluids, vapors, and particulate matter.[3,4] For example, Hou et al. reported a series of liquid-based porous gating systems (LPGSs) suitable for different applications, transforming the basic problems of microporous membranes from a solid−liquid interface to a liquid−liquid interface, which brings more directions to the design of intelligent gating systems.[5−7] More recently, Jiang et al. demonstrated the use of biomimetic ferrofluid-based nanofluids that can facilitate multilevel ultrafast responsive ionic and molecular transport through velocity control. By changing the direction and strength of the external magnetic field, a speed control, ultrafast response molecular transport (<0.1 s), and controllable current gating ratio are achieved.[8] These gating systems can switch between the "ON" or "OFF" status, which

brings more possibilities to the sustained drug release (SDR) design of intelligent gating systems.

Due to the large volume of water contained in the three-dimensional structure, the hydrogel material with excellent biocompatibility has been widely used for SDR in recent years.[9,10] In particular, since the pH-responsive hydrogels show a drastic and reversible volume change upon either swelling or shrinking, they have considerable potential as the materials for SDR in antitumor research.[11,12] For instance, a new chitosan-based hybrid nanogel that in situ immobilizes CdSe quantum dots (QDs) in the chitosan-poly(methacrylic acid) networks has been reported by Zhou et al. These hybrid nanogels have low cytotoxicity and could illuminate the B16F10 cells, sense the environmental pH change, and control the release of drugs molecule in the pH range of 5−7.4.[13] To further increase the storage capacity of the drug, a new type of hydrogel-based porous gating system (HPGS) has been developed for drug
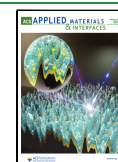
delivery.[14,15] For example, Quan et al. constructed a novel pH-responsive oral drug delivery system by covering mesoporous silica with pH-triggered poly(acrylic acid) (PAAC). In the gastric environment (pH = 2.0), molecules of doxorubicin hydrochloride (Dox) were encapsulated in the pore channels due to the pore exit being sealed with contracted PAAC, but in the colonic environment (pH = 7.6), Dox was rapidly released as the cap was removed.[15] Although many previous works have been devoted to the study of HPGSs in biomedical applications,[4,16] fine control of SDR with artificial HPGSs and the corresponding underlying mechanism are still challenges and an urgent need.

Herein, we reported a kind of bioinspired hydrogel-based porous gating membrane (HPG-MB) composed of the pH-responsive hydrogel as the valve and polydimethylsiloxane (PDMS) as the frame that is fabricated by femtosecond (fs) laser in situ microdrilling and UV exposure.[17] The fs laser can accomplish one-step and maskless fabrication of structures with good expandability and a low thermal effect, which is not possible with a soft lithography or hierarchical mold method.[18−20] A sturdy HPG-MB with a micropore array can be obtained. Due to the merit that hydrogels are sensitive to pH, the HPGS can reversibly close or open the valve to switch between "ON" and "OFF" states according to the expansion or contraction of the hydrogel. By studying the changes in Dox molecular concentration with the transport duration, we rely on the basis of the Korsmeyer−Peppas model to enable the dynamic control of molecular transport. Furthermore, the membrane is further used for the preparation of a drug-containing hydrogel-based porous gating microcapsule (HPG-MC). In a basic environment, the doxorubicin hydrochloride (Dox) molecules were loaded in the capsule because the pore outlets were capped with hydrogel, but in an acid environment, it exhibited SDR because of the opening of the microchannels. Therefore, this HPGS provides an advantageous solution to the difficulties in clinical devices for tumor therapy and shows promising prospects in the designing of controllable DDS technologies in modern medical research.

■ EXPERIMENTAL SECTION

Materials. The commercial polydimethylsiloxane (PDMS) films with PE mask (thickness: 500 μm) were purchased by Bald Advanced Materials Co., Ltd.; acrylic acid, the polymer polyvinylpyrrolidone (PVP, average $M_w \approx 1, 300, 000$), N,N-dimethylformamide (DMF, 99.5%), and triethanolamine (TEA, 99%) were obtained from Sinopharm Chemical Reagent Co. Ltd. 4,4-Bis(diethylamino)-benzophenone (EMK, 97%) and pentaerythritol triacrylate (PETA, 96%) were purchased from Aladdin Reagent (Shanghai) Co. Ltd. All chemicals were used as received.

Femtosecond Laser Fabrication. The microdimple and conical micropore array of polydimethylsiloxane (PDMS) films with a PE mask were fabricated using femtosecond (fs) laser line-by-line scanning. A laser beam (104 fs, 1 kHz, 800 nm) from a regeneratively amplified Ti:sapphire fs laser system (Legend Elite-1 K-HE, Coherent) was used for ablation. During the fabrication process, a galvanometer scanning system (SCANLAB) was used to guide the laser beam on the membrane surface, where the laser beam focused and scanned along the x/y coordinate directions. The scan spacing between two lines was 100 nm. The laser power was 200−400 mW, and the scanning speed was 2 mm·s^{-1}.

Preparation of the AAC Precursor. First, 0.8 mL of acrylic acid (AAC, 99%) and 0.15 g of polyvinylpyrrolidone (PVP, 30 K) were mixed and stirred. Then, 1.5 mL of the above solution was taken, 0.04 mL of pentaerythritol triacrylate (PETA, 98%), 0.5 mL of triethanol-amine (TEA, 99%), and 100 mL of 4,4-bis(diethylamino)

benzophenone (EMK, 97%)/N, N-dimethylformamide (DMF, 99.5%) solution (20 wt %) were added, and then the solution was stirred for 1 h to fully mix the components. Finally, the precursor was kept under yellow light conditions to avoid additional exposure.

Dox and Glucose Transport of pH-Triggered HPG-MB. Dual-cell equipment was used to test the Dox and glucose transport performance at different time points for HPG-MB with the "ON" state at pH = 6.0 and "OFF" state at pH = 8.0. The HPG-MB was fixed in the middle of the H-shaped container and at the interface of the two units. Two cells are filled with the same pH = 6.0 solution or pH = 8.0 solution, but Dox was added into the left volume to form a Dox concentration of 1.72 mmol·L^{-1}. We measure the fluorescence intensity of the released Dox using a spectrofluorometer (F7100 Hitachi, Japan) at an emission wavelength of 590 nm and excitation wavelength of 470 nm. Glucose amounts were monitored by a microplate reader at 550 nm (Thermo Fisher Scientific).

In Vitro pH-Triggered Dox Release. Dox-loaded HPG-MC was added into a glass bottle, which was filled with 10 mL of the solution at pH 6.0 or 8.0. We measure the fluorescence intensity of the released Dox using a spectrofluorometer (F7100 Hitachi, Japan) at an emission wavelength of 590 nm and excitation wavelength of 470 nm.

Cell Culture. HeLa cells were purchased from Alnylam Pharmaceuticals. DMEM medium (Invitrogen) with 10% fetal bovine serum (FBS, Sigma-Aldrich) and 1% penicillin/streptomycin (Sigma-Aldrich) was used to incubate cells in an incubator (Thermo Scientific) at 37 °C with 5% CO$_2$ and 90% relative humidity. The cells were subcultivated approximately every 3 days at 80% confluence using 0.25% (w: v) trypsin at a split ratio of 1:5. All other reagents and solvents are of analytical grade and used without further purification.

In Vitro Cytotoxicity. In vitro cytotoxic viability was assessed by a standard CCK-8 method using HeLa cells. Briefly, 96-well plates were used to seed HeLa cells at an initial density of 5000 cells/well and cells were incubated in 10 mL of DMEM at 37 °C for 24 h. Then, 10 mL of Dox-loaded HPG-MC solutions with different concentrations at different times was added to each well. In order to eliminate the interference of drugs in the detection, it is necessary to set up wells with corresponding amounts of cell culture medium, Dox, and CCK-8 solutions, but no cells were used as blank controls. After culturing for 24 h, 10 μL of CCK-8 solution was added to the cells followed by incubation at 37 °C for an additional 4 h. A spectrophotometric fluorescence spectrophotometer (F7100 Hitachi, Japan) at a test wavelength of 450 nm was used to measure the absorbance of the CCK-8 assay. The relative cell viability was calculated with the equation

$$\text{cell viability } v(\%) = \frac{A_D - A_{b_1}}{A_{b1} - A_{b2}} \times 100\%$$

where A_D is the absorbance value of the medium that containing Dox and cells. A_{b1} is the absorbance value of the control medium containing Dox without cells. A_{b2} is the absorbance value of the blank medium. Experimental group A_D is rendered as average ± SD ($n = 3$).

Apoptosis Assay. 96-well plates were used to seed HeLa cells at an initial density of 5000 cells per well, and cells were incubated in 1 mL of medium containing 10% FBS for 24 h. Subsequently, apoptosis of HeLa cells was induced by different concentrations of Dox in membranes/microcapsules at different periods, and the cells were allowed to incubate for another 4 h. HeLa cells were collected by digestion and centrifugation with EDTA-free trypsin (centrifugation at 2000 rpm for 5 min). After removal of the medium, they were subsequently washed with PBS (pH 7.4) solution three times and 50,000 cells were collected. Binding buffer was added to suspend cells, and 5 μL of Annexin V-FITC and 5 μL of propidium iodide were added to mix well, respectively. The reaction was carried out for 15 min at room temperature and away from light and detected by FACScan (BD Biosciences). The excitation wavelength E_x was 488 nm, and the emission wavelength E_m was 530 nm. The green fluorescence of Annexin V-FITC was detected by the FITC channel, and propidium iodide was detected by other channels. Cells were trypsinized and pooled with the floating cells, and the cells were
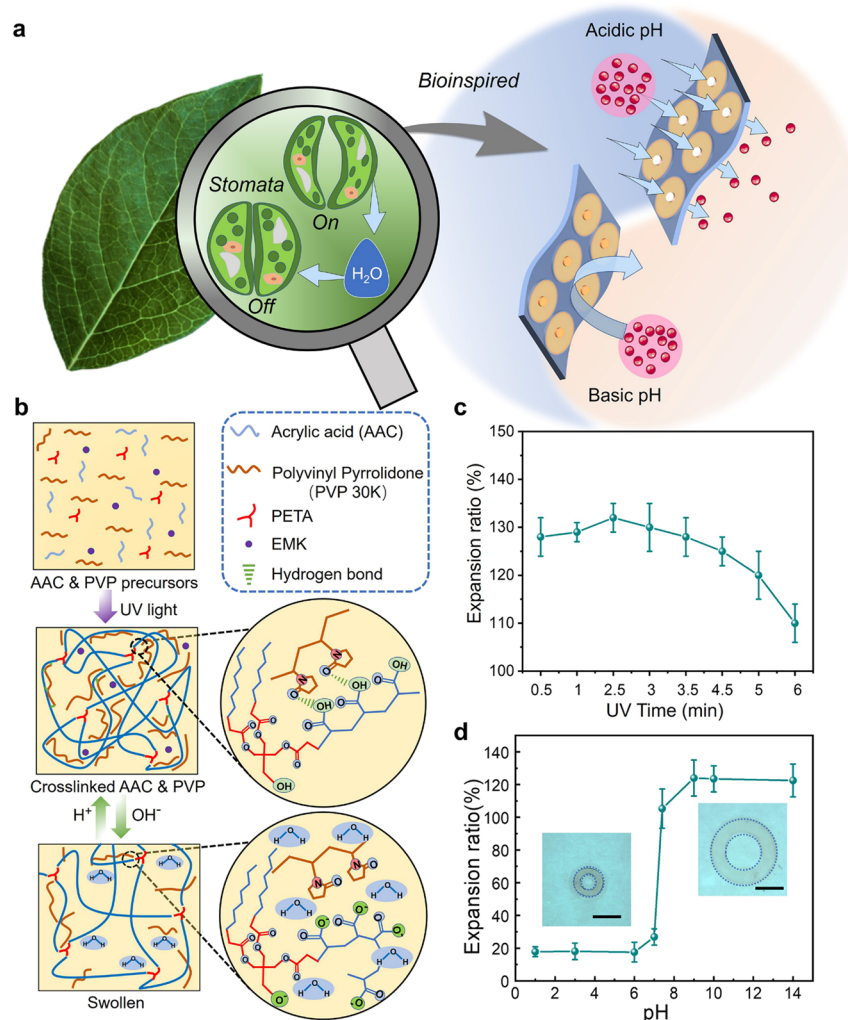
Figure 1. Bioinspired HPGS for molecule transport. (a) Schematic of the stomatal system in a leaf (left), which can control the vapor transport by absorbing or releasing through two guard cells. The bioinspired HPGS is based on the solution pH (right), in which acid solution opens the valve and the basic solution closes the valve. (b) Ultraviolet (UV) polymerization of the hydrogel precursor, which includes acrylic acid (AAC) and polyvinylpyrrolidone (PVP) as the monomer, PETA as the cross-link, and EMK as the photoinitiator. (c) Expansion ratio of the PAAC hydrogel changing with the ultraviolet exposure time. (d) Changes in the expansion ratio of PAAC hydrogel with the pH switching from 1 to 14, scale bar: 20 μm.

collected for flow cytometry quantitative analysis followed by analysis using Modfit 2.0.

    Instruments and Characterization. The scanning electron microscope (SEM) images were taken by a field-emission scanning electron microscope (JSM-6700F). Optical photos were obtained by a digital camera (Canon EDS-60D, Japan) with an alternative macro lens (Canon EF 100 mm f/2.8 L, Japan). The AAC precursor was exposed to ultraviolet (UV) light (UVP high-intensity B-100 series lamp, 21, 700 mW·cm^{-2}) for 0.5 to 6 min to solidify; the wavelength for UV curing is 365 nm. An electrokinetic analyzer (SurPASS[3] Eco instruments) was used to measure the zeta potential of the membrane.

RESULTS AND DISCUSSION

    Bioinspired HPGS. Figure 1a shows that the two guard cells can control transpiration and gas exchange by absorbing or desorbing water in a plant leaf. Inspired by the stomata in the plant leaf (left),[21,22] we synthesized a pH-responsive and speed-controlled HPGS for ion and molecular transport. The bioinspired HPGS driven by pH stimuli enables small molecular (glucose/Dox) transport on-demand (right). According to the reported method, we optimized the

preparation of the hydrogel precursor, which consists of pH-responsive acrylic acid (AAC) and polyvinylpyrrolidone (PVP) (Figure 1b). When the solution pH was increased above the ionization threshold (pH = 7), the electrostatic repulsion between the carboxylate ions repelled other acidic pendant groups on the AAC, resulting in a significant swelling of the hydrogel (Figure 1b). As shown in Figure S1, we obtained different thicknesses of hydrogel membranes when the UV exposure time was varied from 0.5 to 6 min. The maximum hydrogel thickness of ~420 μm was obtained in an exposure time of 5 min. The presence of micropores resulted in a lower strength with the thinnest hydrogel layer compared to the control sample of blank PDMS. Then, with the increase of the hydrogel thickness, the strength of the hybrid film was tuned in the stiffness range of 1.69−3.13 MPa (Figure S2). The density of 3D cross-linked networks of hydrogels increased with the UV exposure time. When the density of hydrogel networks is higher, the electrostatic repulsion forces to repel other molecular chains become larger, resulting in a significant decrease in the expansion ratio of the hydrogel (Figure 1c).
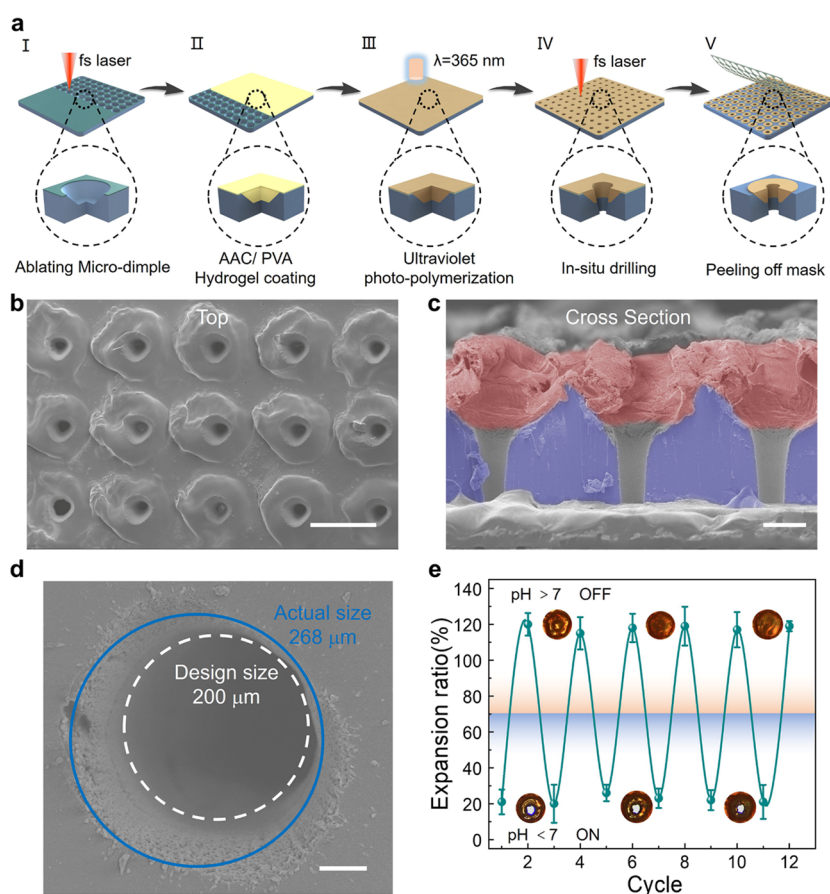
Figure 2. Fabrication and characteristic of the HPG-MB. (a) Fabrication of HPG-MB, (I) Fabrication of the frame layer. A series of regular circular microdimples are fabricated on the PDMS polymer with a mask by the femtosecond laser ablation method. (II,III) Fabrication of the valve layer. The precursor hydrogel is poured into the microdimple on the surface of PDMS. Then, the membrane is exposed to UV light for 5 min to cure the hydrogel with a 420 μm layer. (IV) The smaller tapered hole in the center of the microdimple is drilled in situ by a femtosecond laser. (V) Tearing off the mask attached at the beginning. (b) Top and cross-sectional view of the scanning electron microscope (SEM) image for HPG-MB, scale bar: 500 μm. (c) Cross-sectional view of the SEM image for HPG-MB, scale bar: 200 μm. (d) With a laser power of 300 mW, the actual diameter of the aperture is about 1.34 times larger than the design size, scale bar: 50 μm. (e) Repetition test of the HPG-MB expanding/contracting cycles between the "OFF" and "ON" states. The inset shows the image of pores in the above two states at different cycles.

To obtain an ideal gating effect, we set out UV exposure time for 5 min to form a hydrogel thickness of about 420 μm and the expansion ratio is nearly 120%. The definition of the expansion ratios is shown in Figure S3. As shown in the inner images of Figure 1d, the relationship between expansion ratio and the solution pH value is measured by testing the outer diameter of the hydrogel ring structure. The acidic expansion ratio measured in our experiments is about 20%, and the alkaline expansion ratio is ~120%. In the pH < 6 solution, there is only a little change in the expansion ratio of the hydrogel ring structure, which sharply increases as the pH value increases from 6 to 8. The expansion ratio remained at ~120% when the solution pH > 8. Thus, these expansion properties of pH-responsive hydrogels enable realizing the HPG-MB.

Fabrication and Properties of the HPG-MB. This HPG-MB consists of a hydrogel valve and a frame: the former is made of pH-responsive hydrogels and the latter consists of the PDMS film. Those two structures are bonded by UV polymerization. By designing the dimensions of the valve and the frame, we are able to flexibly control the open/close states of the valve depending on the pH of the surrounding microenvironment. Inspired by the Janus hybrid membrane structure for draining blood and biological fluids around the wound in our previous work,[23] we design a similar structure but use pH-responsive hydrogels to control the ON/OFF state of the micropores (Figure 2a). A commercial PDMS film with a PE mask was used in the following steps. Then, microdimple arrays were fabricated on PDMS by the fs laser ablation method, which can serve as containers for hydrogel.[24] By reducing the processing power of the laser, these dimples will be shallower than the dimples we reported in previous work[23] because it is better to control the ON/OFF state of the micropores. After cleaning the surface with an air gun, the hydrogel precursor was applied to the surface of the film before it was exposed to UV light. The mask was then peeled off from the edge of the membrane with a tweezer to obtain the multifunctional HPG-MB. By using the laser parameter of 0.75 μJ pulse energy and 2 mm·s^{-1} scanning speed, this membrane was successfully drilled in situ to obtain conical micropores. The SEM images (Figure 2b,c) from the top and cross section show the valve and frame structure for the two components. The SEM images with higher magnification (Figure S4) did not show an obvious 3D network or porous structure on the surface of the hydrogel. This may be due to the self-smoothing effect induced by the fs laser on the hydrogel surface. Fourier-transform infrared (FTIR) spectra show that the characteristic absorption bands at 1723 cm^{-1} may be the absorption of
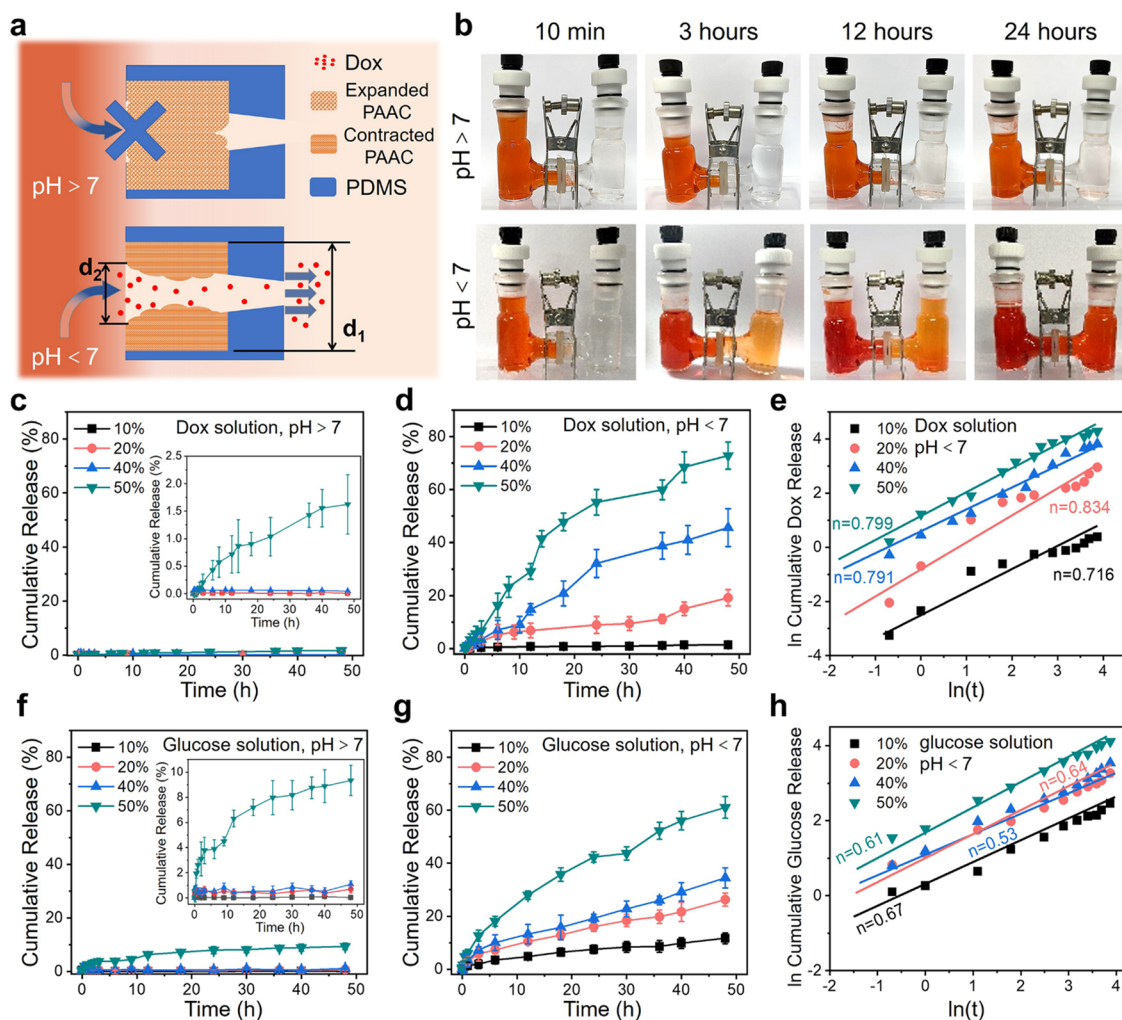
Figure 3. Speed-controlled molecular transport and underlying release mechanism. (a) Schematics of the gating performance of the membranes for drug molecule transport. The aperture ratio is shown as d_2/d_1 where aperture d_1 is the diameter of microdimple and d_2 is the diameter of micropores drilled by the laser. (b) Photos of a dual-cell for the Dox diffusion tests at different time points for HPG-MB with the "ON" state at pH < 7 and "OFF" state at pH < 7. (c) In pH > 7 solution, the cumulative Dox release curve within 48 h at different aperture ratios (d_2/d_1) from 10% to 50%. (d) In pH < 7 solution, the cumulative Dox release curve within 48 h at different aperture ratios (d_2/d_1) from 10% to 50%. (e) Korsmeyer−Peppas mechanism curves for Dox release with different aperture ratios (d_2/d_1). (f) In pH > 7 solution, the cumulative glucose release curve within 48 h at different aperture ratios (d_2/d_1) from 10% to 50%. (g) In pH < 7 solution, the cumulative glucose release curve within 48 h at different aperture ratios (d_2/d_1) from 10% to 50%. (h) Korsmeyer−Peppas mechanism curves for glucose release with different aperture ratios (d_2/d_1).

carboxyl groups of PAAC (Figure S5). We can assign the bands at 1551 and 1407 cm^{-1} to asymmetric and symmetric stretching vibrations of COO$^-$ anion groups, respectively.[15,25]

A decrease in zeta potential from 1.89 mV at solution pH = 3 to −6.19 mV at solution pH = 9 indicates that the isoelectric point of PAAC is about 4 to 5 (Figure S6). However, the addition of PVP in our formulation directly affects the expansion ratio of the hydrogel through the interaction of the hydrogen bonding, which causes the gap between the pH of expansion ratio change and the isoelectric point for our hydrogel membrane. To visualize the switchable gating of the HPG-MB, Rhodamine-B dyes are grafted to the PAAC hydrogels and the expanded or contracted hydrogel is measured by a real-time confocal microscope. In the solution of pH > 7, the hydrogel valves expanded along the plane covering the porous surface. The red fluorescence shrinks, and the area of the micropore surface becomes larger in the solution at pH < 7 (Figure S7). When the laser power is 300 mW for the vertical drilling process, the actual size of the

aperture would be about 1.34 times larger than the design one due to the thermal effects of laser ablation, and there were no obvious ablation parts on the hydrogel surface (Figure 2d). To further validate the repetitive performance of the HPG-MB, the expansion ratio is measured with multiple expansion and contraction cycles. During the cycle tests, all samples were allowed to stay in the solution for at least 1 min to ensure sufficient expansion or contraction of the hydrogel part. The hydrogel in the dimple around the micropores retained their shape even after six expansion and contraction cycles (Figure 2e). As a result, we have successfully constructed a bioinspired intelligent membrane with excellent pH response gating performance and good cycle stability in different pH solutions, which is beneficial for the further study of speed-controlled molecular and ion transport.

Speed-Controlled Molecular Transport and Underlying Release Mechanism. Figure 3a shows schematic illustrations of the gating performance of the membranes for drug molecule transport. The aperture ratio (d_2/d_1) is defined
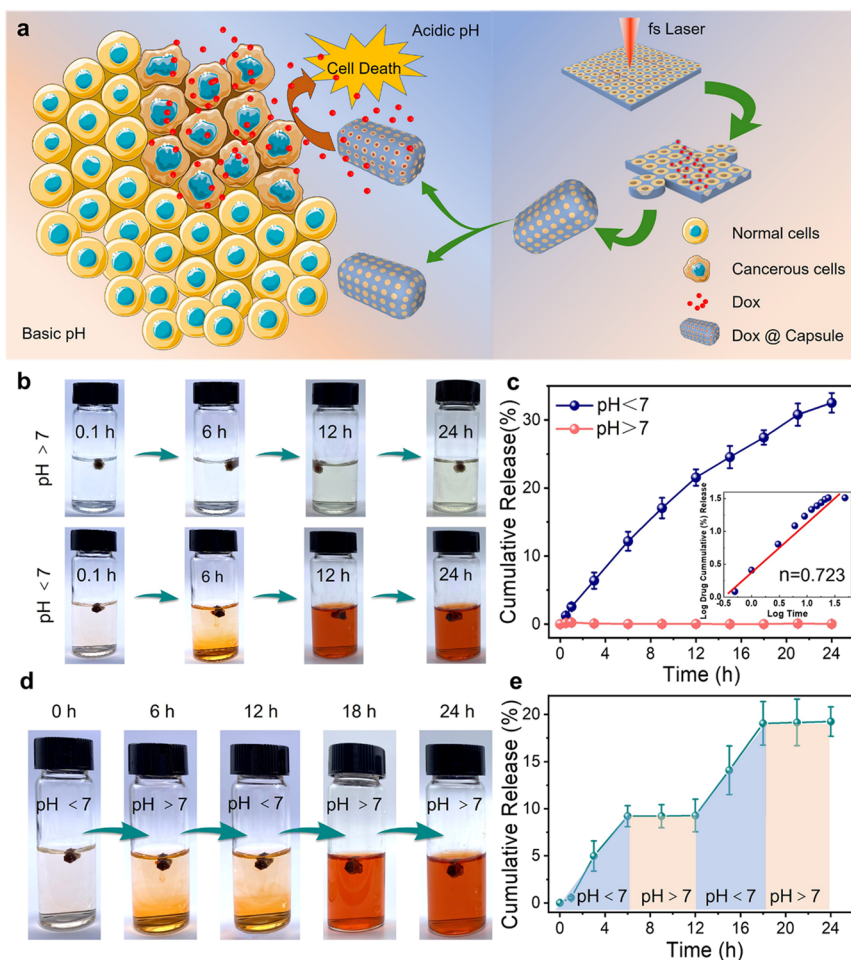
Figure 4. HPG-MC for DDS. (a) Schematic showing the design of a pH-triggered HPG-MC for anticancer drug release beside the cancer cell. (b) Photos of the Dox diffusion tests of the microcapsule at 0.1, 6, 12, and 24 h for Dox release in pH < 7 solution and Dox obstruction in pH > 7 solution, respectively. (c) Time-resolved release profiles of Dox from microcapsule in different pH solutions. The inset shows the fitting lines based on Korsmeyer–Peppas Model for the Dox release. (d,e) Different states are combined to obtain an on-demand drug delivery curve and images over time.

as the ratio between the diameter of the conical pore and the diameter of the microdimples. To verify the gating capability of the HPG-MB, liquid-phase diffusion experiments were used with an "H" cell configuration as a tracker. It was separated by the HPG-MB and divided into two pools, a seed pool (Dox solution) and a diffusion pool (water solution with different pH values). For the diffusion pool with pH > 7 solution (upper row in Figure 3b), the expansion of PAAC blocked the pore entrances of the valve–frame composite in the closed state of HPG-MB. Consequently, almost no color change is observed in the right pool. When the diffusion pool is loaded with pH < 7 solutions, the opened state of the valve–frame rendered Dox accessible to the conical pores, and the Dox molecule can diffuse from the seed pool into the diffusion pool easily. After 24 h, there is no difference in the red color of Dox between the two pools (lower row in Figure 3b). Then, we compared the transport speed at different pH variations from 5.0 to 9.0 in Figure S8. We can see that the transport speed is almost the same when the solution pH is 6 and 5. Also, the amount of DOX released is approximately 0% in pH > 7 solution, which is consistent with the results of the sharp change in the expansion ratio in pH = 7 solution for our hydrogels in Figure 1d.

With the increase of the d_2/d_1 from 10% to 50%, the corresponding crossover concentration of Dox in the diffusion

pool grows from 1.47% to 72.80% at 48 h in pH < 7 solution (Figure 3d). Meanwhile, the cumulative release speed gradually rose with the rising diameter of composite micropores. For comparison, the cumulative concentration curve of Dox underwent barely visible changes from 0.05% to 1.62% in pH > 7 solutions (Figure 3c), and the release of Dox is negligible until $d_2/d_1 > 40\%$. The low area ratio of the pores (~9%) on the membrane lead to much fewer intrinsic three-dimensional micropores in our membrane than that in the pure hydrogel membrane system. Thus, the amount of Dox released is approximately 0% in pH > 7 solution. Confocal images of switchable gating micropores at $d_2/d_1 = 50\%$ show that the micropores cannot be fully covered in pH > 7 solution due to the limited expansion rate of the hydrogel (Figure S9). These results suggest that the PAAC layers could effectively obstruct the transport of Dox when d_2/d_1 is less than 40%.

In order to better understand the drug release mechanism and predict drug release in vitro, drug release kinetics are increasingly being studied.[11] Normally, Korsmeyer–Peppas and Higuchi release models are considered to study the drug release mechanism and kinetic for hydrogel materials.[26−29] Equations of the kinetic models are given in Figure S10, and the parameters' values are presented in Table S1. The linear correlation coefficients (R^2) are the evaluation criteria when
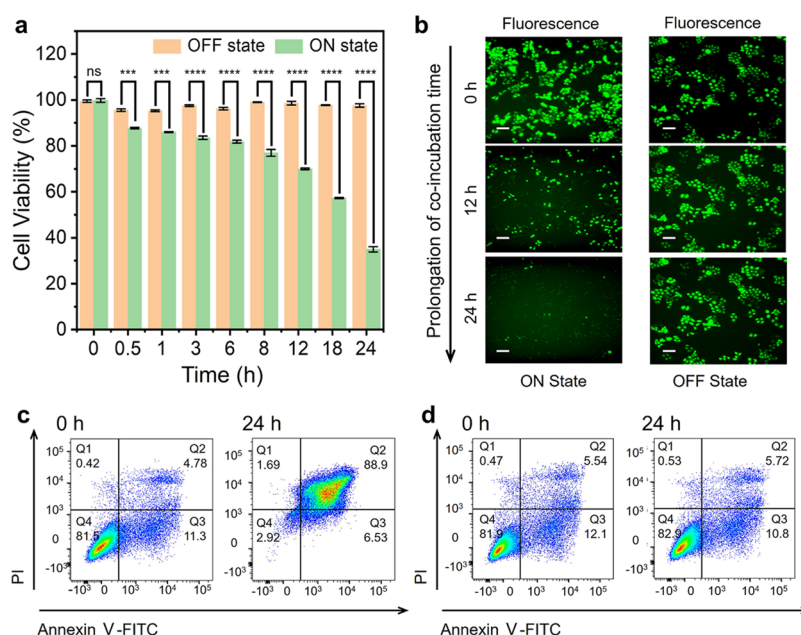
Figure 5. In vitro antitumor strategy for SDR mediated by the HPG-MC. (a) In vitro cytotoxicity of HPG-MC in pH > 7 and pH < 7 incubation with HeLa cells. Data are presented as mean STD ($n = 3$, two-tailed Student's t-test: *$P \leq 0.05$, **$P \leq 0.01$, ***$P \leq 0.001$, ***$P \leq 0.0001$). (b) Representative CLSM microimages show three-time points of GFP fluorescence in cells (green) incubated with pH < 7 solution (left) and pH > 7 solution (right), where Dox was released after 24 h by the microcapsule. The scale bar represents 40 μm. (c,d) Flow cytometric analysis of HeLa cell apoptosis induced with HPG-MC at 0 and 24 h. The left image shows Dox release with Annexin V-FITC/propidium iodide (PI) staining in pH < 7 solution and the right image shows drug obstruct in pH > 7 solution. The lower-left (Q3), lower-right (Q4), upper-right (Q1), and upper-left (Q2) quadrants in each panel indicate the populations of normal, early apoptotic, late apoptotic, and necrotic cells, respectively.

considering whether the model is more suitable. The linear correlation coefficients (R^2) of the Higuchi model are lower than that of Korsmeyer–Peppas model with different aperture ratios. Thus, we choose Korsmeyer–Peppas model to define the release of the drug. The Korsmeyer–Peppas model also describes some release mechanisms, such as water diffusion into the matrix, swelling of the matrix, and dissolution of the matrix. The value of diffusion constant (n) gives the underlying release mechanism, $n = 0.43$ for typical Fickian diffusion, $n = 0.85$ for erosion transport, and $0.43 < n < 0.85$ for a combination of Fickian and erosion transport behavior, which is defined as non-Fickian diffusion.[30] Here, the values of n for different d_2/d_1 are all larger than 0.43 but smaller than 0.85 (Figure 3e and Table S1), which indicates non-Fickian diffusion behaviors. In other words, the expansion process of the hydrogel combined with the diffusion through micro-porous media leads to the 'non-Fickian' diffusion behavior.[31] The results show that the transport of Dox is synergistically driven by the concentration gradient of Dox, the external pH stimuli, and the structure of PAAC on the surface of the valve–frame composite. Analyzing the amount of Dox released at fixed time points, we constructed a calibration curve of Dox fluorescence vs corresponding concentration to get an accurate idea of the concentration of drug diffused in the lower chamber (Figure S11).[32]

The same situation can be observed when Dox is switched with a smaller molecule such as methylene blue dye (Figure S12) and glucose. Consistent with Dox diffusion experiments, the cumulative release curve of glucose from the open states of HPG-MB in pH < 7 rose from 11.68% to 61.08% at 48 h (Figure 3g) with increasing d_2/d_1. In contrast, they are only from 0.02% to 0.68% from 10% to 40% in pH > 7 solutions (Figure 3f). It is worth noting that the pH-responsive PAAC

layers could not effectively obstruct the transport of glucose when d_2/d_1 is greater than 40% either in pH > 7 solution (Figure 3g). It is mainly because the expansion ratio of the hydrogel is limited, which leads to the pores in the valve–frame not being completely blocked by the hydrogel, so there is a slow release of glucose compared to the closed state of HPG-MB. In addition, the calculated n value is also greater than 0.43 with d_2/d_1 increasing from 10% to 50% in pH < 7 solutions according to the non-typical Fickian diffusion (Figure 3h). The quantity of glucose is taken by an emission wavelength of 550 nm, and the absorbance value is converted into the glucose concentration according to the standard curve (Figure S11).[33] In general, these results suggest the possibility of designing comprehensive molecular transport systems that both are speed-controlled and enable the reversible gated flow of multiphase substances. More importantly, the non-typical Fickian mechanism of drug release from HPG-MB for the SDR is conducive to speed procedural control.

HPG-MC for SDR. To better realize the concept based on switchable gating of the membrane to the microcapsule of 3D entity functionalization assemblies, Figure 4a describes the programmed microcapsule process, which is developed for high-performance operable and controllable SDR. This HPG-MC is composed of HPG-MB for hosting small molecules (Dox), and the weakly acid tumor microenvironment (TME) led to the located release of Dox molecules. The desired two-dimensional plane diagram of microcapsules was cut with a femtosecond laser ablation method, and the bonding agent (liquid PDMS) was applied to connect neighboring parts on the edge of the shape for encapsulating anticancer drugs or other substances.

An ideal system for SDR could be created by the HPG-MC, which will not cause any leakage without an applied stimulus.

The drug release from the microcapsule (~2 mg Dox powder) was determined in the weakly acidic solution and the weakly basic solution at room temperature. As Figure 4b shows, the color of the buffer solution has not changed significantly in "ON" states of HPG-MC (pH > 7), indicating that the Dox encapsulated on the microcapsule is almost nonexistently released. Also, the Dox loaded in the microcapsule is released with the opening of the valve of the HPG-MC (pH < 7), together with the color of the solution changing to deep red in 24 h. As the blue line shows in Figure 4c, a continuous increase to 32.5% Dox released is observed after 24 h in "ON" states. A control experiment with a red line in Figure 4c shows that almost none of the Dox is released during the same period in a pH > 7 solution (Figure 4c, Figure S13). In addition, the inset illustrating fitting lines are based on the Korsmeyer−Peppas model in the switchable "ON" states, while $n = 0.78$ indicates that the release of Dox molecules obeys the non-typical Fickian mechanism. As shown in Figure 4d,e, ~9% Dox is released in a pH < 7 solution for 6.0 h, with evidence of color change of the solution. Next, when the pH value of the solution changes to a weakly basic environment (pH > 7), the valves are closed and the release of Dox is arrested immediately; the color of the Dox solution will not change obviously. Then, the further release of Dox can be achieved by decreasing the solution pH value to less than 7, as evidenced by the color of the solution turning red. Usually, cancerous tissues have a pH of about 5.8−7.0, while non-cancerous tissues have a pH of about 7.5. As a result, the HPG-MC shows outstanding drug loading capacity, accelerating release in tumor tissue and inhibiting release in normal tissues, providing drug release stability, as well as showing excellent biocompatibility.

In Vitro Antitumor Strategy for SDR Mediated by the HPG-MC. Three levels including flow cytometry, cell viability, and in vitro antitumor strategies were further assessed with HeLa cervix to observe the antitumor effect of HPGS.[34] The cytotoxicity of released Dox solution in switchable states by Dox-loaded HPG-MC toward HeLa cells was evaluated with a CCK-8 assay (Figure 5a).[35] All bare solutions of different pH values are non-toxic to HeLa cells (Figure S14), and the cell viability was all dependent on both the released Dox by HPG-MC and incubation time of cell culture. With the extension of the actual release time of the "ON" state, the viability of the HeLa cells gradually decreased. However, HeLa cells with HPG-MC in the "OFF" state showed negligible cytotoxicity with prolonged release time within the detection concentration range. In addition, we qualitative assessed the release of Dox by confocal laser scanning microscopy (CLSM) and apoptosis of cancer cells through changes in the green fluorescent protein signal. The HeLa-GFP cells were incubated with released Dox solution in the "ON" state of HPG-MC, and Figure 5b shows that the fluorescence intensity gradually weakens, while fluorescence intensity stays at the same level when the HeLa-GFP cells were incubated under the same treatment with the "OFF" state (pH > 7) (Figure S15). Next, Annexin V-FITC/pyridine iodide apoptosis detection was performed to compare the apoptosis-inducing capabilities of the released Dox solution in the "ON" state (pH < 7) with the released Dox solution in the "OFF" state (pH > 7) from HPG-MC at different times.[36] Annexin V-FITC labels the phosphatidylserine translocated to the extracellular membrane at the onset of apoptosis, while pyridine iodide as the nucleic acid fluorescent dye could pass through the cell membrane of dead cells and dye the nucleus red. This combination allows differentiation between early apoptotic cells, late apoptotic cells, and living cells, which can be quantitatively determined by flow cytometry. The total apoptotic ratio of HeLa cells incubated with Dox solution from the "ON" state of HPG-MC can actually reach 88.54%, which is significantly higher than the final 10.23% of apoptotic ratio with Dox solution from the "OFF" state of HPG-MC (Figure 5c,d).[37,38] According to the above analysis, the results confirmed that the Dox-loaded HPG-MC is an effective intercellular delivery vehicle, which can enhance the apoptosis-inducing activity.

◼ CONCLUSIONS

The bioinspired HPGS including membrane (HPG-MB) and microcapsules (HPG-MC) were successfully fabricated based on a femtosecond laser ablation and UV polymerized method. By controlling the pH of the environment, the deformations of the PAAC hydrogel on the PDMS were highly adjustable, and thus a quick response, controllable, and long-term cycling system with a high ratio was achieved. Theoretical analysis and experimental data demonstrate that the HPGS is achieved through a rational valve−frame interface design. Finally, benefitted from the versatility of this pH-triggered membrane, We introduce this HPG-MB into drug molecule release applications and the HPG-MC is capable of achieving on-demand tumor cell treatment by controllable speed and reversible switch gating. This HPGS (HPG-MB/HPG-MC) has hopeful applications for the treatment of digestive cancer such as colon cancer, stomach cancer, and other cancer diseases.

◼ ASSOCIATED CONTENT

ⓢ Supporting Information

The Supporting Information is available free of charge at https://pubs.acs.org/doi/10.1021/acsami.2c07319.

> SEM images of different thicknesses of the PAAC layer at different UV exposure times; stress−strain curve of the different thickness hydrogel layers under tension; schematic illustration of the size changes of the hydrogel in different environments; SEM images with higher magnification for the membrane; FT-IR spectra of PDMS and the PAAC-covered PDMS membrane; zeta potential of the membrane; confocal images of switchable gating membrane; cumulative Dox release curve within 48 h at different pH solutions; confocal images of switchable gating micropores at $d_2/d_1 = 50\%$; fitting of experiment data to Korsmeyer−Peppas and Higuchi models; concentration standard curve of Dox and glucose; Images of a dual-cell for the methylene blue dye diffusion tests; DOX diffusion concentration of HPG-MC at 24 h for drug release; cell fluorescence activity and cell viability at different times in different pH solutions; representative CLSM microimages of three-time points of GFP fluorescence, bright field and merge; release kinetic parameters obtained from non-linear fitting plots of Korsmeyer−Peppas and Higuchi models (PDF)

◼ AUTHOR INFORMATION

Corresponding Authors

Bingrui Liu − *CAS Key Laboratory of Mechanical Behavior and Design of Materials, Department of Precision Machinery and Precision Instrumentation, University of Science and*

Technology of China, Hefei, Anhui 230027, China; ⓘ orcid.org/0000-0002-1245-0338; Email: brliu@ ustc.edu.cn

Zuojun Shen − *Department of Clinical Laboratory, The First Affiliated Hospital of USTC Division of Life Sciences and Medicine, University of Science and Technology of China, Hefei, Anhui 230027, China;* ⓘ orcid.org/0000-0001-7052-5652; Email: zuojunshen@ustc.edu.cn

Authors

Juan Zhang − *Department of Clinical Laboratory, The First Affiliated Hospital of USTC Division of Life Sciences and Medicine, University of Science and Technology of China, Hefei, Anhui 230027, China*

Chao Chen − *School of Materials Science and Engineering, Hefei University of Technology, Hefei 230009, China;* ⓘ orcid.org/0000-0002-8061-0292

Shaojun Jiang − *CAS Key Laboratory of Mechanical Behavior and Design of Materials, Department of Precision Machinery and Precision Instrumentation, University of Science and Technology of China, Hefei, Anhui 230027, China*

Yiyuan Zhang − *CAS Key Laboratory of Mechanical Behavior and Design of Materials, Department of Precision Machinery and Precision Instrumentation, University of Science and Technology of China, Hefei, Anhui 230027, China;* ⓘ orcid.org/0000-0002-0393-2597

Bing Xu − *School of Mechanical Engineering, Suzhou University of Science and Technology, Suzhou 215009, China*

Ang Li − *Department of Clinical Laboratory, The First Affiliated Hospital of USTC Division of Life Sciences and Medicine, University of Science and Technology of China, Hefei, Anhui 230027, China;* ⓘ orcid.org/0000-0002-6816-7064

Junchao Xu − *Department of Clinical Laboratory, The First Affiliated Hospital of USTC Division of Life Sciences and Medicine, University of Science and Technology of China, Hefei, Anhui 230027, China*

Dawei Wang − *CAS Key Laboratory of Mechanical Behavior and Design of Materials, Department of Precision Machinery and Precision Instrumentation, University of Science and Technology of China, Hefei, Anhui 230027, China*

Leran Zhang − *CAS Key Laboratory of Mechanical Behavior and Design of Materials, Department of Precision Machinery and Precision Instrumentation, University of Science and Technology of China, Hefei, Anhui 230027, China*

Yanlei Hu − *CAS Key Laboratory of Mechanical Behavior and Design of Materials, Department of Precision Machinery and Precision Instrumentation, University of Science and Technology of China, Hefei, Anhui 230027, China;* ⓘ orcid.org/0000-0003-1964-0043

Jiawen Li − *CAS Key Laboratory of Mechanical Behavior and Design of Materials, Department of Precision Machinery and Precision Instrumentation, University of Science and Technology of China, Hefei, Anhui 230027, China;* ⓘ orcid.org/0000-0003-3950-6212

Dong Wu − *CAS Key Laboratory of Mechanical Behavior and Design of Materials, Department of Precision Machinery and Precision Instrumentation, University of Science and Technology of China, Hefei, Anhui 230027, China;* ⓘ orcid.org/0000-0003-0623-1515

Jiaru Chu − *CAS Key Laboratory of Mechanical Behavior and Design of Materials, Department of Precision Machinery and Precision Instrumentation, University of Science and*

Technology of China, Hefei, Anhui 230027, China; ⓘ orcid.org/0000-0001-6472-8103

Complete contact information is available at:
https://pubs.acs.org/10.1021/acsami.2c07319

Author Contributions

The manuscript was written through contributions of all authors. All authors have given approval to the final version of the manuscript.

Notes

The authors declare no competing financial interest.

■ REFERENCES

(1) Yang, Y.-W.; Sun, Y.-L.; Song, N. Switchable Host−Guest Systems on Surfaces. *Acc. Chem. Res.* **2014**, 47, 1950−1960.

(2) Zhang, B.; Korolj, A.; Lai, B. F. L.; Radisic, M. Advances in organ-on-a-chip engineering. *Nat. Rev. Mater.* **2018**, 3, 257−278.

(3) Zarzar, L. D.; Kim, P.; Aizenberg, J. Bio-Inspired Design of Submerged Hydrogel-Actuated Polymer Microstructures Operating in Response to pH. *Adv. Mater.* **2011**, 23, 1442−1446.

(4) Kim, H.; Kim, K.; Lee, S. J. Nature-inspired thermo-responsive multifunctional membrane adaptively hybridized with PNIPAm and PPy. *NPG Asia Mater.* **2017**, 9, e445−e445.

(5) Chen, B.; Zhang, R.; Hou, Y.; Zhang, J.; Chen, S.; Han, Y.; Chen, X.; Hou, X. Light-Responsive and Corrosion-Resistant Gas Valve with Non-Thermal Effective Liquid-Gating Positional Flow Control. *Light Sci. Appl.* **2021**, 10, 127.

(6) Hou, X.; Hu, Y.; Grinthal, A.; Khan, M.; Aizenberg, J. Liquid-Based Gating Mechanism with Tunable Multiphase Selectivity and Antifouling Behaviour. *Nature* **2015**, 519, 70−73.

(7) Sheng, Z.; Zhang, J.; Liu, J.; Zhang, Y.; Chen, X.; Hou, X. Liquid-Based Porous Membranes. *Chem. Soc. Rev.* **2020**, 49, 7907−7928.

(8) Wang, C.; Wang, D.; Miao, W.; Shi, L.; Wang, S.; Tian, Y.; Jiang, L. Bioinspired Ultrafast-Responsive Nanofluidic System for Ion and Molecule Transport with Speed Control. *ACS Nano* **2020**, 14, 12614−12620.

(9) Zhang, A.; Jung, K.; Li, A.; Liu, J.; Boyer, C. Recent Advances in Stimuli-Responsive Polymer Systems for Remotely Controlled Drug Release. *Prog. Polym. Sci.* **2019**, 99, No. 101164.

(10) Wang, H.; Mu, Q.; Revia, R.; Wang, K.; Zhou, X.; Pauzauskie, P. J.; Zhou, S.; Zhang, M. Chitosan-Gated Magnetic-Responsive Nanocarrier for Dual-Modal Optical Imaging, Switchable Drug Release, and Synergistic Therapy. *Adv. Healthcare Mater.* **2017**, 6, 1601080.

(11) Wibowo, F. R.; Saputra, O. A.; Lestari, W. W.; Koketsu, M.; Mukti, R. R.; Martien, R. pH-Triggered Drug Release Controlled by

Poly (Styrene Sulfonate) Growth Hollow Mesoporous Silica Nanoparticles. *ACS Omega* **2020**, *5*, 4261−4269.

(12) Das, S.; Subuddhi, U. pH-Responsive Guar Gum Hydrogels for Controlled Delivery of Dexamethasone to the Intestine. *Int. J. Biol. Macromol.* **2015**, *79*, 856−863.

(13) Wu, W.; Shen, J.; Banerjee, P.; Zhou, S. Chitosan-Based Responsive Hybrid Nanogels for Integration of Optical pH-Sensing, Tumor Cell Imaging and Controlled Drug Delivery. *Biomaterials* **2010**, *31*, 8371−8381.

(14) Su, H.-L.; Xu, L.; Hu, X.-J.; Chen, F.-F.; Li, G.; Yang, Z.-K.; Wang, L.-P.; Li, H.-L. Polymer Grafted Mesoporous SBA-15 Material Synthesized via Metal-Free ATRP as pH-Sensitive Drug Carrier for Quercetin. *Eur. Polym. J.* **2021**, *148*, No. 110354.

(15) Tian, B.; Liu, S.; Wu, S.; Lu, W.; Wang, D.; Jin, L.; Hu, B.; Li, K.; Wang, Z.; Quan, Z. pH-Responsive Poly (acrylic acid)-Gated Mesoporous Silica and Its Application in Oral Colon Targeted Drug Delivery for Doxorubicin. *Colloids Surf., B* **2017**, *154*, 287−296.

(16) Kim, J.; Im, S.; Kim, J. H.; Kim, S. M.; Lee, S. M.; Lee, J.; Im, J. P.; Woo, J.; Moon, S. E. Artificial Perspiration Membrane by Programmed Deformation of Thermoresponsive Hydrogels. *Adv. Mater.* **2020**, *32*, 1905901.

(17) Xu, B.; Li, A.; Wang, R.; Zhang, J.; Ding, Y.; Pan, D.; Shen, Z. Elastic Janus Film for Wound Dressings: Unidirectional Biofluid Transport and Effectively Promoting Wound Healing. *Adv. Funct. Mater.* **2021**, *31*, 2105265.

(18) Hu, Y.; Yuan, H.; Liu, S.; Ni, J.; Lao, Z.; Xin, C.; Pan, D.; Zhang, Y.; Zhu, W.; Li, J.; Wu, D.; Chu, J. Chiral Assemblies of Laser-Printed Micropillars Directed by Asymmetrical Capillary Force. *Adv. Mater.* **2020**, *32*, 2002356.

(19) Jiang, S.; Hu, Y.; Wu, H.; Zhang, Y.; Zhang, Y.; Wang, Y.; Zhang, Y.; Zhu, W.; Li, J.; Wu, D.; Chu, J. Multifunctional Janus Microplates Arrays Actuated by Magnetic Fields for Water/Light Switches and Bio-inspired Assimilatory Coloration. *Adv. Mater.* **2019**, *31*, 1807507.

(20) Yang, L.; Mayer, F.; Bunz, U. H.; Blasco, E.; Wegener, M. Multi-Material Multi-Photon 3D Laser Micro-and Nanoprinting. *Light: Adv. Manuf.* **2021**, *2*, 1−17.

(21) Hetherington, A. M.; Woodward, F. I. The Role of Stomata in Sensing and Driving Environmental Change. *Nature* **2003**, *424*, 901−908.

(22) Lundgren, M. R.; Mathers, A.; Baillie, A. L.; Dunn, J.; Wilson, M. J.; Hunt, L.; Pajor, R.; Fradera-Soler, M.; Rolfe, S.; Osborne, C. P.; Sturrock, C. J.; Gray, J. E.; Mooney, S. J.; Fleming, A. J. Mesophyll Porosity is Modulated by the Presence of Functional Stomata. *Nat. Commun.* **2019**, *10*, 1−10.

(23) Zhang, J.; Liu, B.; Liu, X.; Wang, D.; Dong, B.; Zhang, Y.; Xu, B.; Chen, C.; Shen, Z. Laser Ablated Janus Hydrogel Composite Membrane for Draining Excessive Blood and Biofluid around Wounds. *Macromol. Mater. Eng.* **2022**, *2200026*, 2200026.

(24) Xiong, W.; Zhou, Y.; Hou, W.; Jiang, L.; Mahjouri-Samani, M.; Park, J.; He, X.; Gao, Y.; Fan, L.; Baldacchini, T.; Silvain, J. F.; Lu, Y. Laser-Based Micro/Nanofabrication in One, Two and Three Dimensions. *Front. Optoelectron.* **2015**, *8*, 351−378.

(25) Sohail, K.; Khan, I. U.; Shahzad, Y.; Hussain, T.; Ranjha, N. M. pH-sensitive polyvinylpyrrolidone-acrylic acid hydrogels: Impact of material parameters on swelling and drug release. *Braz. J. Pharm. Sci.* **2014**, *50*, 173−184.

(26) Ritger, P. L.; Peppas, N. A. A Simple Equation for Description of Solute Release II. Fickian and Anomalous Release from Swellable Devices. *J. Controlled Release* **1987**, *5*, 37−42.

(27) Jain, A.; Jain, S. K. In Vitro Release Kinetics Model Fitting of Liposomes: An Insight. *Chem. Phys. Lipids* **2016**, *201*, 28−40.

(28) Higuchi, T. Mechanism of Sustained-Action Medication. Theoretical Analysis of Rate of Release of Solid Drugs Dispersed in Solid Matrices. *J. Pharm. Sci.* **1963**, *52*, 1145−1149.

(29) Siepmann, J.; Peppas, N. A. Higuchi Equation: Derivation, Applications, Use and Misuse. *Int. J. Pharm.* **2011**, *418*, 6−12.

(30) Pu, X. Q.; Ju, X. J.; Zhang, L.; Cai, Q. W.; Liu, Y. Q.; Peng, H. Y.; Xie, R.; Wang, W.; Liu, Z.; Chu, L. Y. Novel Multifunctional Stimuli-Responsive Nanoparticles for Synergetic Chemo-Photothermal Therapy of Tumors. *ACS Appl. Mater. Interfaces* **2021**, *13*, 28802−28817.

(31) Gorban, A. N.; Sargsyan, H. P.; Wahab, H. A. Quasichemical Models of Multicomponent Nonlinear Diffusion. *Math. Model. Nat. Phenom.* **2011**, *6*, 184−262.

(32) Tatiana, A. S.; Marina, N. K.; Ekaterina, V. A.; Kirill, G. L.; Gennady, A. M.; Victor, B. L. Attenuation Correction Technique for Fluorescence Analysis of Biological Tissues with Significantly Different Optical Properties. *Front. Optoelectron.* **2020**, *13*, 360−370.

(33) Li, J.; Yao, Y.; Jiang, L.; Li, S.; Zhang, W. Time-Domain Terahertz Optoacoustics: Manipulable Water Sensing and Dampening. *Adv. Photon.* **2021**, *3*, No. 026003.

(34) Nogueira-Librelotto, D. R.; Scheeren, L. E.; Macedo, L. B.; Vinardell, M. P.; Rolim, C. M. pH-Sensitive Chitosan-Tripolyphosphate Nanoparticles Increase Doxorubicin-Induced Growth Inhibition of Cervical HeLa Tumor Cells by Apoptosis and Cell Cycle Modulation. *Colloids Surf., B* **2020**, *190*, No. 110897.

(35) Tan, L.; Yang, M. Y.; Wu, H. X.; Tang, Z. W.; Xiao, J. Y.; Liu, C. J.; Zhuo, R. X. Glucose- and pH-responsive Nanogated Ensemble Based on Polymeric Network Capped Mesoporous Silica. *ACS Appl. Mater. Interfaces* **2015**, *7*, 6310.

(36) Vermes, I.; Haanen, C.; Steffens-Nakken, H.; Reutellingsperger, C. A Novel Assay for Apoptosis Flow Cytometric Detection of Phosphatidylserine Expression on Early Apoptotic Cells using Fluorescein Labelled Annexin V. *J. Immunol. Methods* **1995**, *184*, 39−51.

(37) Zhao, X.; Guo, K.; Zhang, K.; Duan, S.; Chen, M.; Zhao, N.; Xu, F. J. Orchestrated Yolk−Shell Nanohybrids Regulate Macrophage Polarization and Dendritic Cell Maturation for Oncotherapy with Augmented Antitumor Immunity. *Adv. Mater.* **2022**, *34*, 2108263.

(38) Zhu, Y.; Lin, M.; Hu, W.; Wang, J.; Zhang, Z. G.; Zhang, K.; Yu, B.; Xu, F. J. Controllable Disulfide Exchange Polymerization of Polyguanidine for Effective Biomedical Applications by Thiol-Mediated Uptake. *Angew. Chem., Int. Ed.* **2022**, No. e202200535.